Preprint
UCRL-JC-145037

A Comparison of Ultrasound Tomography Methods in Circular Geometry

R. R. Leach Jr., S.G. Azevedo, J. G. Berryman, H. R. Bertete-Aguirre, D. H. Chambers, J. E. Mast, P. Littrup, N. Duric, S. A. Johnson, F. Wuebbeling

This article was submitted to
Medical Imaging 2002, San Diego, CA., February 23-28, 2002

January 24, 2002

U.S. Department of Energy
Lawrence Livermore National Laboratory

This work was performed under the auspices of the United States Department of Energy by the University of California, Lawrence Livermore National Laboratory under contract No. W-7405-Eng-48.

A comparison of ultrasound tomography methods in circular geometry

*Richard R. Leach Jr. [a], Stephen G. Azevedo [a], James G. Berryman [a],
Hugo R. Bertete-Aguirre [a], David. H. Chambers [a], Jeffrey. E. Mast [a],
P. Littrup [b], Neb. Duric [c], Stephen. A. Johnson[d], Frank. Wuebbeling [e]

[a]Lawrence Livermore National Laboratory, Livermore, CA 94550, [b]Karmanos Cancer Institute, Detroit, MI 48201, [c]Department of Physics and Astronomy, University of New Mexico, [d]University of Utah, [e]University of Muenster)

ABSTRACT

Extremely high quality data was acquired using an experimental ultrasound scanner developed at Lawrence Livermore National Laboratory using a 2D ring geometry with up to 720 transmitter/receiver transducer positions. This unique geometry allows reflection and transmission modes and transmission imaging and quantification of a 3D volume using 2D slice data. Standard image reconstruction methods were applied to the data including straight-ray filtered back projection, reflection tomography, and diffraction tomography. Newer approaches were also tested such as full wave, full wave adjoint method, bent-ray filtered backprojection, and full-aperture tomography.

A variety of data sets were collected including a formalin-fixed human breast tissue sample, a commercial ultrasound complex breast phantom, and cylindrical objects with and without inclusions. The resulting reconstruction quality of the images ranges from poor to excellent.

The method and results of this study are described including like-data reconstructions produced by different algorithms with side-by-side image comparisons. Comparisons to medical B-scan and x-ray CT scan images are also shown. Reconstruction methods with respect to image quality using resolution, noise, and quantitative accuracy, and computational efficiency metrics will also be discussed.

Key Words: Ultrasound tomography, experimental ultrasound scanner, transducer geometry, image reconstruction, qualitative and quantitative acoustic parameters

1. INTRODUCTION

Imaging remains one of the most powerful tools in modern medical diagnosis. This study is primarily concerned with applying new ultrasound imaging methods to detect cancerous tissue in the human breast. Currently, the two leading mammography technologies include x-ray mammography machines and medium resolution ultrasound devices. X-ray mammography remains the predominant tool by producing images with very high (.03mm) resolution. It is also routinely used to detect and guides biopsy of malignant calcifications. However, there are many drawbacks to using x-ray technology including non-direct detection of tumors, ionizing radiation is required, a highly trained operator is needed, the procedure can be very uncomfortable, and only transmission mode signals are used. Medium resolution ultrasound relieves some of these drawbacks as tumors are directly imaged, there is little discomfort, and no ionizing radiation is used. However the resolution of this technology (~2mm.) and the use of reflection mode signals exclusively often produce low-quality images with speckle and shading artifacts. In addition, neither approach provides direct quantitative tissue identification. Improved tissue characterization could result in a reduction of the estimated one million benign biopsies performed each year in the United States (Liberman[1], 2000), costing up to several billion dollars (Secker-Walker[2], et. al., 1999). For example, the majorities of breast calcifications are benign and comprise ~ 80% of stereotactic biopsies guided by mammography (Makoske[3], et. al., 2000). High resolution, quantitative tissue characterization could potentially clearly identify benign masses thereby obviating the need for biopsies in such cases.

* author contact information – leach1@llnl.gov, 1 925 423-3351, Lawrence Livermore National Laboratory, 7000 East Avenue, L-541, Livermore, CA 94550, USA

The Ultrasound Breast Imaging Project in the Medical Technologies Program and Engineering Directorate at Lawrence Livermore National Laboratory (LLNL) has been developing advanced ultrasound tomography systems for diagnostic breast cancer detection over the last three years. The project was sponsored by the Karmanos Cancer Institute (KCI) under the Computerized Ultrasound Risk Evaluation (CURE) program. The goals of this project are to produce high resolution (<1.0mm) 2.5 to 3D quantitative ultrasonic images of human breast tissue by using transmission and reflection modes. 2.5 to 3-D visualization will afford better understanding of morphology and location of tissue features. High quality data sets would be generated. The system would provide direct imaging of tumors, no discomfort, no ionizing radiation, and would not require a highly trained operator. Another important goal of the project was to research, develop, and test the best-known tomographic algorithms and determine their efficacy and applicability. For example, the classic straight-ray filtered back projection algorithm (Kak[4], et. al., 1988) is a proven method for x-ray applications, but how well would this straight ray assumption work in this high-resolution acoustic application? The following sections will describe the methodology, data, algorithms, results, conclusions, and recommendations resulting from this work.

2. METHODOLOGY

2.1 Scanning System

LLNL has built an ultrasound scanning system designed to simulate virtually any transducer array design. The system has six degrees of freedom and has been optimized for signal-to-noise (SNR), pulse shape, minimization of systematic errors, and automated preprocessing. In this system, both a transmitting and receiving transducer are used. The two transducers are placed close together and at the same height and at the same distance from the object to be scanned. Waveforms are then transmitted and captured in this configuration. The receiving transducer is then moved using one of the rotational stages and data is again gathered. This process is continued until the receiver has gathered data at all desired incremental angular receiver positions. This process is then repeated whereby the transmitter is also moved incrementally using one of the rotational stages and waveforms are once again gathered for all receiver positions. This continues until the desired volume of the object has been scanned. This is a time consuming process taking several hours, and producing large amounts of data. For example for several of the objects scanned, incremental angular transducer position was 1 degree and typically 100mm from the object. Using a 1.5 MHz. Frequency (2us pulses) each transducer pair location captured approximately 2.7ms of data. In this case, the total storage for all transceiver locations is about 1Gbytes for each slice. This data is then used to reconstruct an image. For a more detailed description of the scanner and signal conditioning, see (Azevedo[5], et. al., 2002) in these proceedings.

2.2 Scanned Objects

The first tests objects (phantoms) were used to model mass margins and evaluate resolution (Figure 2.2.1). The first three phantoms built by TechniScan, Inc. are numbered TP110, TP111, and TP112. Each is a cylindrical shaped phantom 40mm in diameter by about 150mm and filled with Agar, N-propanol, and H_20 proportioned to attain an internal sound speed of ~1.54mm/μs. The phantoms are housed with a Latex (condom) casing. TP110 has no inclusions. TP111 has 5 pairs of nylon wires (.2mm diameter) running the length of the phantom with pair spacing from 2 to 5mm. The pairs form a pentagon whose vertices are ~12.5mm from center of phantom. TP112 has 2 added inclusions (1mm latex tubes) running the length of the phantom and filled with a water/alcohol mixture. As seen in Figure 2.2.1(d), TP112 developed an outer crack, which worsened progressively over time. Also seen in the figure is the transducer pair in the scanning tank. The phantoms were typically oriented in the tank in this manner, scanning cross sections at one or more levels through the test object. The next text object is a commercial ultrasound silicon based breast phantom (BB1S) where small, high-contrast inclusions were placed (injected) within the material. The final object is a normal cadaveric human breast placed in formalin and sealed in a 100mm diameter, cylindrical container with fiducial nylon wires running the length of the outside of the container at four locations (quadrants).

2.3 Performance Specifications

Image performance in this project is measured by the ability to ultimately demonstrate, in a complex object, high resolution, quantifiable images. This goal is described by three major specifications. The first two specifications require differentiation of 0.1% variation in sound speed and 3.0% variation in attenuation within the object. The system

could then detect subtle attenuation and sound speed magnitude variations comparable to the magnitude of the differences between cyst fluid and adjacent normal breast tissue.

The third resolution goal of the scanning system was to image sub-millimeter (<0.5 mm) features in breast tissue using both reflection and transmission scanning modes. Fourier sampling theory states that a function or object must be sampled at an interval no larger than half the smallest scale of variation. This is equivalent to the reciprocal of twice the highest frequency to be completely reconstructed with no error and is the minimum sampling required. To meet the performance goals, the scanner used a frequency of 1.5 MHz. with 2 μs pulses. This allowed best penetration of the objects while retaining sub-mm spatial resolution. For man-made scan objects incremental transducer spacing was set at 1 degree at a scan radius of 100 mm. For the breast tissue and the commercial breast phantom, the radius was increased to 150 mm to accommodate the larger sized object. Also, for the complex breast tissue sample, the incremental receiver spacing was decreased to 0.25 degree. Unfortunately, an adequate discussion of digital sampling theory is beyond the scope of this paper. For a more complete treatment of this topic, interested readers are referred to (Azevedo[6], 1991)' (Degroot[7], et. al., 1987), (Dudgeon[8], et. al., 1984), and (Natterer[9], 1986).

3. DATA

Scans were taken for each of the phantoms TP110, TP111, and TP112 with 360 transmitter and 320 receiver positions. Slice data was also acquired for the BTS1 phantom at 9 different heights spaced at 10mm. The BTS1 tissue container was scanned for a total of 14 different levels at 5mm vertical spacing. This data was taken for 180 transmitter and 1601 receiver positions. Each scan was performed in circular geometry. Data quality from the scanning system is in general very reliable. (Azevedo[5], et. al., 2002).

In addition, images were acquired using a clinical ultrasound unit (GE Logic 600) for each of these objects. Finally, a clinical CT scanner (GE Lightspeed Quad detector array) was used to obtain 128 slices from the BTS1 tissue container at ~1.25mm thickness.

4. ALGORITHMS

There exists today a large body of tomographic algorithms, both new approaches and well-tested designs that had been developed over many years. Producing high-resolution quantitative ultrasound images could require a highly accurate underlying model to the extent that might render the method computationally impractical. Modern computer speeds, data storage, and realization of a useful device might demand algorithmic compromises and modifications. With this in mind the LLNL data sets were applied to a host of algorithms that can be loosely catagorized into the following four methods..

4.1 Filtered back projection (FBP) methods.

Straight-ray, or projection tomography reconstructs object from properties summed along straight lines through the object as described in the well-known study by Kak and Slaney[4]. This approach is sometimes called geometric optics and works well when the transmitted energy travels in a straight or near-straight path through the scanned object from transmitter to receiver. Adequate spatial sensor placement using this algorithm produces extremely high-quality images and will produce both slowness and attenuation data throughout the object. This algorithm works well with x-ray energy as seen in CT scanning machines. However, for ultrasound applications the straight-ray assumption is violated as the transmitted energy is diffracted, reflected, and scattered as it passes through complex object. The straight ray filtered back projection (SRFBP) was applied to some of the earlier data for comparison value. The result is reconstructed images with poor resolution and a high amount of distortion (smearing).

With the goal of reducing the distortion, a new algorithm was developed at LLNL by Berryman[10], which assumed the rays were not straight, but slightly bent within some bounds. This bent ray filtered back projection (BRFBP) algorithm was also applied to some of the data. Both these methods are desirable as they have the advantage relatively fast computational speed when compared to other (full-wave) approaches.

4.2 Full-aperture tomographic (FAT) methods.

Our full aperture tomography (FAT) algorithm allows circumferential processing of reflection and transmission data. An extension of reflection mode imaging, or so-called "B-scans" currently used in medical ultrasound, FAT produces images that highlight scattering sources in the insonified object. It assumes the wave scattering is isotropic and sound speed in the medium is known or calculable. The method is analogous to synthetic aperture radar (SAR) or delay-and-sum beam forming techniques[11]. FAT models the object to be imaged as a collection of point scatterers. A linearizing assumption is made that acoustic energy scattered by each individual point object does not scatter off other point

scatterers. This assumption of ignoring multiple scattering allows one to formulate the imaging solution for a single point scatterer independent of all other point scatterers. Then, the solution involving all point scatters becomes the linear superposition of the result from each individual point scatterer. The scattered signal from a given point in the object is sampled around the aperture (circular or paddle geometry) scanned by the receiving transducer. Assuming the point scatters isotropically, it effectively becomes a secondary point source. Thus, the goal of the imaging method is to determine the location of the point source given the data collected around the aperture.

4.3 Diffraction tomographic (DT) methods.

Diffraction tomography (DT) is based upon the Bourne approximation to acoustic scattering and is a simplified version of a method previously used (Andre[12], et. al., 1997) in a circular array system. This algorithm assumption that scattering is weak throughout the scanned object for a given wavelength. The result is that in areas where scattering does occur produces artifacts such as speckling and ringing. The DT method used is performed largely in the Fourier domain and is a non-iterative process, resulting in very fast computation times. For a more detailed description of the application of diffraction tomography and its performance in cylindrical geometry, see (Chambers[13], et. al., 2002) in these proceedings.

4.4 Full-wave reconstruction methods.

The most accurate, yet computationally expensive algorithms use complete or nearly complete solutions to the acoustic wave equation. Using the full wave (amplitude and phase) of the measured field, these algorithms perform and full inversion to reconstruct the properties of the medium. The algorithm used in this study is described in the U. S. patent by Johnson[14], et. al. A second full-wave algorithm method using adjoint fields was also applied in this study. This reconstruction method, called the full-wave adjoint method is described in a paper by Dorn[15], et. al. These algorithms promise to have the highest quantitative accuracy, but are burdened by high computational requirements.

4.5 Leading Algorithms

Research and development of reconstruction algorithms require both high quality and high efficiency as seen in figure 4.5.1. Using the scanner data to evaluate reconstructed images has narrowed the focus to the four most promising algorithms. First the FAT algorithm produces some of the highest quality images. Currently FAT provides no quantitative data, however a quantitative version of the algorithm (QFAT) is near completion. Images will be shown in the next section for FAT reconstructions. Secondly, the DT algorithm is most promising for the high-speed computational capability, on the order of hundreds of times faster than other leading methods. Third, the FW algorithm clearly provides the best quantitative results as well as also producing some of the highest quality images. Finally, The FWA algorithm is nearing completion, but can currently produce images and will also be shown in the next section.

5. RESULTS AND DISCUSSION

In this section image reconstruction results are shown for TP111, TP112, BB1s, and BTS1 test objects. In each case a side-by-side comparison is shown of various reconstruction methods and when available, a comparison to the GE Logic 600 B-scan unit. Finally, a remarkable comparison between a FAT slice reconstruction of BTS1 and the GE Lightspeed Quad detector array (CT scanner) is shown.

5.1 TP111 Reconstructions

The standard measurement for resolution in this study is a measure of the full-width half maximum (FWHM) value of a point spread function (PSF) comparison of a reconstructed image and it's the ground truth. For example the TP110 phantom is a cylinder 40mm in diameter with a known sound speed. An image is first created with precisely these specifications. A reconstructed image is compared to this image by calculating the Weiner estimate of the PSF. The more accurate the image edges match the model, the narrower the PSF spread and FWHM value. For TP111, the .2mm wires in the TP111 phantom were also used to measure algorithm performance with this resolution metric. Table 5.1.1 shows the results of these measurements. Currently only the FAT algorithm has achieved sub-milimeter performance for the TP110 and TP111 data sets.

Algorithm	FWHM of PSF (λ)	FWHM of PSF (mm)
SRFBP (velocity)	3.3	2.5
SRFBP (attenuation)	4.1	3.1
BRFBP (velocity)	3.3	2.5
FAT	0.57	0.43
FW	1.7	1.3

Table 5.1.1 The Weiner estimate of the point spread function (PSF) was measured using the phantom edges in the TP110 phantom or the nylon wires in the TP111 phantom. From this function, the full-width half maximum (FWHM) was calculated to proved a resolution metric for each algorithm. Comparison shows FBP algorithms have a higher PSF. FAT performed the best with sub λ performance.

The TP111image reconstruction results seen in figure 5.1.1 support this as the FAT image (d) has the sharpest wires indicating that small details in tissue might be seen best using this algorithm. However, since FAT currently is not scaled to any physical quantity, the high-contrast wires dominate the image and the edge of the phantom is weakly seen. The FW image (f) has a slightly lower resolution, but does a much better job of showing all edges and has produced very accurate sound speed values in this image.

The B-scan image (b) shows the high-contrast wires quite well, however artifacts and distortion is high due to bright speckling throughout the image as well as streaking and shadowing. The DT image (e) result is very good as it requires minimal computation and is only slightly affected by diffraction effects. SRFBP in (c) is clearly a poor result illustrating typical image distortion as a result of the straight-ray assumption.

5.2 TP112 Reconstructions

The TP112 image reconstruction results shown in figure 5.2.1 show that the B-scan machine (b) does produce an image showing the two inclusions, however the speckling, bright spots and shadowing amount to increased presence of artifacts and higher levels of distortion as seen previously. The DT image (c) illustrates the typical ringing artifacts at the edges of the phantom where there is often a high degree of scattering, however the inclusions are clearly seen. The FAT image (d) again has a superior contrast, clearly showing the edges of the inclusion. The FW (e) image also shows very high quality results for the inclusions.

Close examination of the center inclusion in the reconstruction what appears to be a fold in the latex lining is seen (d, e). This was unknown when the data was taken, but post-examination of the phantom revealed that the fold did exist and thus confirmed the measurement. Also, The outer inclusion (c, d, e) appears to have a protruding tab (at 4'oclock). Investigating this feature revealed a real crack over the length of the phantom that had been developing (see figure 2.2.1f), again supporting the accuracy of the reconstruction results. Furthermore, the crack grew progressively worse. This growth was also detected in the image reconstructions. The DT image data (c) was taken at a later date than the data in (d) and (e). This slice was also slightly higher in the phantom than the previous data. Not only did the image show the growth of the crack, but also the fold on the inner inclusion was not present. This was due to the fact that the fold did not exist throughout the entire length of the inclusion. These details further support the efficacy and usefulness of these methods for analyzing complex objects with high resolution.

5.3 BB1S Reconstructions

The BB1S image reconstruction results shown in figure 5.3.1 were taken using a standard commercial breast phantom with small, high-contrast inclusions inserted into the material. Ground truth in this case was more difficult since the insertion of the material was not done with any high degree of accuracy. The typical method to find the inclusions was to hold the phantom up to a bright light and determine their approximate location.

The B-scan machine was a challenge to locate inclusions, but by using the "hunt and peck" method, the inclusions could eventually be located as seen in (b). A highly trained operator would probably be able to do better, but unfortunately the images had a great deal of speckle distortion, typical of reflection-only tomographic methods. Also shown in (c) is a SRFBP reconstruction of a slice near the base of the phantom. Despite the low resolution and image smearing, an inclusion can be clearly seen.

The FAT images again clearly outperformed as the inclusions were easily found in this slice (d) as well as other slices. A second undetected inclusion in (d) was also found in this slice using the FAT algorithm. Also, note what appear to be stretch marks along the border of the phantom. This is due to the fact that this particular slice was taken near the base of the phantom and what is seen is the glue at the edges, which adheres the BB1S phantom to the base plate.

5.4 BTS1 Reconstructions

The first attempt to image highly complex tissue is shown in Figure 5.4.1. The scanning object (BTS1) was a cadaveric breast that was placed in formalin and sealed in a 100mm diameter cylindrical container (a). In addition, the container was put into a plastic bag and tied at the top. Visually inspection and examination of CT scan images of the tissue in the container show that it appears to be folded such that for a cross-sectional slice, the tissue would form roughly a 'C' shape within the image (b).

In this configuration, the B-scan machine was nearly useless as it was difficult to acquire any reasonable image (c) of the tissue in the container. The DT image (d) was also very poor, however the container edge is discernable as well as the 'knot' in the plastic bag. The FW and FAT algorithms (e, f) were much improved as the container edge, plastic bag, and the 'C' shape of the tissue could be seen. None of the images showed the fiducial markers (nylon wires running the length of the container at the 4 quadrants) or much discernable detail.

The plastic bag was removed and the container was again scanned and images were reconstructed using the FAT algorithm. Figure 5.4.2 illustrates the results. The fiducial markers are clearly seen. Resolution is on the order of <=1mm. Tissue details are clearly visible. The 'C' shape outline of the tissue is now obvious. Also note the areas in the image where no tissue exists (formalin solution) are free of artifacts and highly homogeneous.

The BTS1 phantom was scanned using a clinical CT scanner (GE Lightspeed Quad detector array) The 128 scans were done at 1.25mm thickness. Figure 5.4.3 shows a side-by-side comparison of a 150 by 150 mm segment of the FAT reconstruction (a) with the corresponding CT scan slice (b). Similarities of the tissue shape and boundaries in the striation patters are remarkable.

6. CONCLUSIONS AND RECOMMENDATIONS

Can ultrasound provide a better way to image the human breast in order to detect cancerous tissue? The results of this study are certainly not conclusive, but are both promising and encouraging. Leading tomographic methods in circular geometry as well as images from leading clinical machines have been applied, measured, compared, and competed. Performance metrics are computational costs, image quality, resolution and quantitative accuracy. The result is four leading algorithms, full aperature tomograpy, diffraction tomograpy, full-wave, and full-wave adjoint methods.

Method	Compute time/speed	Resolution	Image quality	Comments / status
Quantified full aperture tomograpy (QFAT)	Medium	High (<1mm)	Very good	LLNL transmission & reflection
Diffraction tomograpy (DT)	Very fast	High (<1mm)	Good	Transmission & reflection
Full-wave tomography (FW)	Slow	High (<1mm)	Very good	Transmission & reflection (proprietary)
Full-wave adjoint tomography (FWA)	Slow	High (<1mm)	Medium	In development
Current ultrasound (B scan machines)	Very fast	Medium (2.0mm)	Poor	Reflection only
X-ray mammography (CT scan machines)	Very fast	Very high (0.03mm)	Good	Dense tissue only

Table 6.1 Image quality versus computational efficiency.

Most of what was presented in this study is highly qualitative. Table 6.1 offers a subjective summary of performance criteria. A combination of algorithms is likely in real clinical devices due to inherent trade-offs. For example, faster algorithms may be used for a global initial analysis or detection, while computationally expensive methods may be used for local discrimination, treatment, or tissue characterization.

More study is needed to provide reliable, quantifiable sound speed and attenuation images of breast tissue. Continued development of full wave algorithms to increase speed and reduce computer requirements is recommended. Further development of the quantifiable version of the FAT algorithm is also recommended. Future work should focus on quantification of sound speed and attenuation measurements coupled with improved design of experiments and data collection.

ACKNOWLEDGEMENTS

This research was work performed under the auspices of the U.S. Department of Energy by the Lawrence Livermore National Laboratory under Contract W-7405-ENG-48. I would like to thank Michael Berggren of Techni-Scan, Inc. for the use of their phantoms and for their reconstructions, Dr. John Boone at U.C. Davis Medical center for the X-ray CT images, Steve Benson and Mick Werve assistance with scanner and data collection efforts. I would like to also thank Steve Azevedo, William Lennon, Jim Candy, and Dave Chambers for their many helpful comments.

REFERENCES

1. Liberman L. *Clinical management issues in percutaneous core breast biopsy.* Radiol Clin North Am. 2000; 38:791-807.
2. Secker-Walker RH, Vacek PM, Hooper GJ, Plante DA, Detsky AS. *Screening for breast cancer: time, travel, and out-of-pocket expenses.* J Natl Cancer Inst 1999, 91:702-8.
3. Makoske T, Preletz R, Riley L, Fogarty K, Swank M, Cochrane P, Blisard D. *Long-term outcomes of stereotactic breast biopsies.* Am Surg. 2000, 66:1104-8.
4. Kak A. C., Slaney M. *Principles of Computerized Tomographic Imaging.* IEEE Press, New York, 1988.
5. Azevedo S., Moore T. L., Huber R. D., Ferguson, W., Leach R. R., Benson S. E. *Apparatus for Circular Tomographic Ultrasound Measurements.* SPIE Medical Imaging Proceedings, 2002
6. Azevedo S. G. *Model-Based Computed Tomography for Nondestructive Evaluation.* LLNL-Report, UCRL-LR-106884, 1991
7. Degroot A. J., Johanssson E. M., Fitch J. P., Grant C. W., Parker S. R. *SPRINT – The systolic processor with a reconfigurable interconnection network of transputers*, IEEE transactions on Nuclear Science, Vol. NS-34, No. 4, pp. 873-877, August 1987
8. Dudgeon D., Mersereau R. *Multidimensional Digital Signal Processing.* New Jersey:Prentice-Hall, 1984.
9. Natterer F. *The Mathematics of Computerized Tomography.* Wiley, Chinchester, 1986
10. J. G. Berryman, *Stable iterative reconstruction algorithm for noninear traveltime tomography*, Inverse Problems, 6, 21-42 (1990).
11. Fitch, J. P., *Synthetic Aperture Radar*, Springer-Verlag, 1988.

12. André MP, Janee HS, Martin PJ, Otto GP, Spivey BA, Palmer DA. *High-speed data acquisition in a diffraction tomography system employing large-scale toroidal arrays.* International Journal of Imaging Systems and Technology 1997; 8:137-147.

13. Chambers D., Littrup, P. *Ultrasound imaging using diffraction tomography in cylindrical geometry*, SPIE Medical Imaging Proceedings, 2002.

14. Johnson S. A., Borup, D. T., Wiskin J. W., Natterer F., Wuebbling F., Zhang Y., Olsen C. *Apparatus and Method for Imaging with Wavefields using Inverse Scattering Techniques.* United States Patent 6,005,916 (1999)

15. Dorn O, Bertete-Aguirre H., Berryman J G and Papanicolaou G C, *A nonlinear inversion method for 3D-electromagnetic imaging using adjoint fields Inverse Problems* V15 pg1523-1558, (1999).

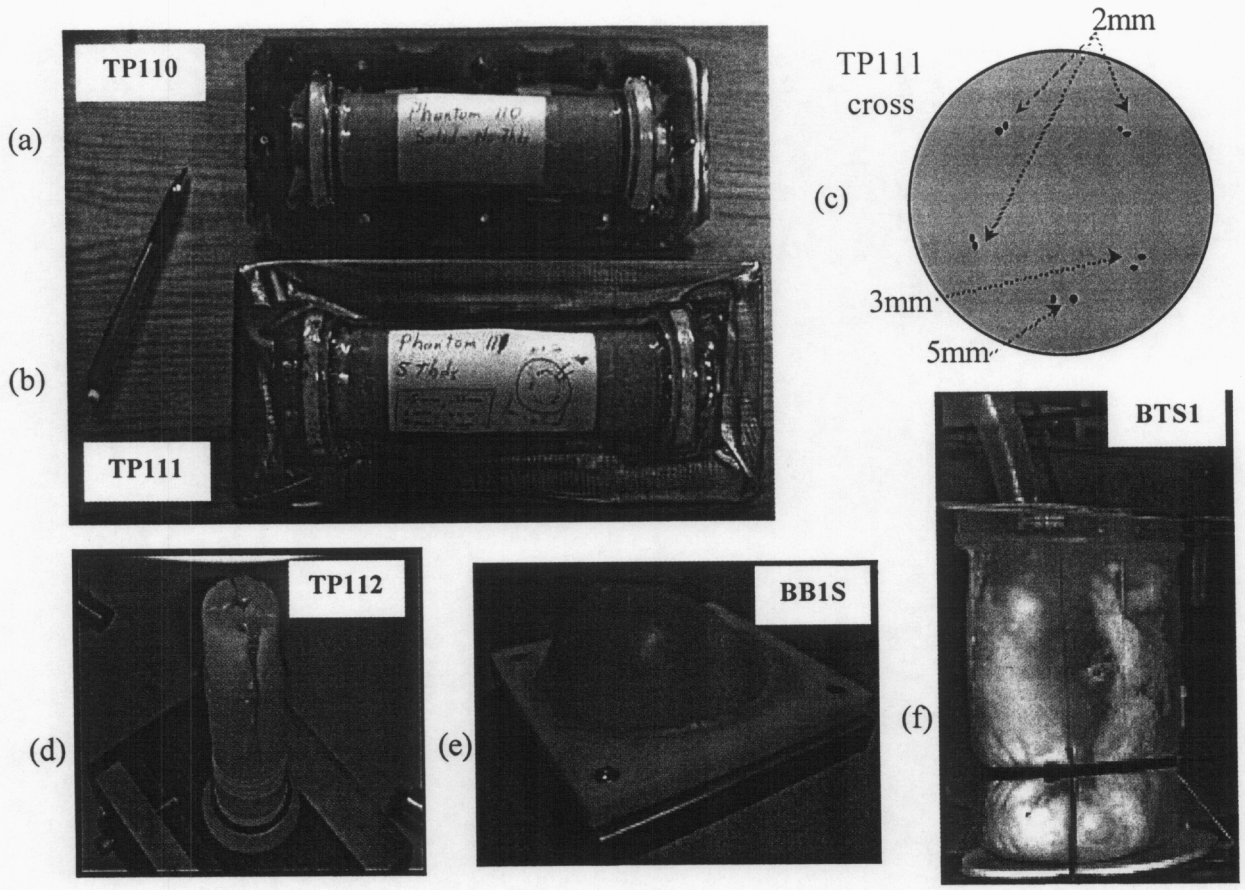

Figure 2.2.1 (a) TP110 phantom 40mm diameter by 140mm in length, filled with Agar, N-propanol, and H_20 which has sound speed of ~1.54mm/μs, housed with a Latex (condom) casing. TP111 phantom (b) is identical to TP110 except slightly longer (180mm) and has 5 pairs of nylon wires (0.2mm diameter fishing line) running the length of the phantom. Each pair is spaced from 2 to 5mm as seen in (c). Cross section of TP111 phantom (c) with 5 pentagonal pairs of wires spaced as shown at a radius of ~12.5mm from center of phantom. TP112 phantom (d) is the same as TP111 except it has no wires, but does have 2 added inclusions (10mm latex tubes) running the length of the phantom and filled with a water/alcohol mixture. As seen, TP112 developed an outer crack which worsened progressively over time. BB1s (e) is a commercial ultrasound silicone based breast phantom where insertion of inclusions is possible. BTS1 (f) is a normal cadaveric human breast placed in formalin and sealed in a 100mm diameter, cylindrical container with fiducial nylon wires running the length of the outside of the container at 4 locations (quadrants).

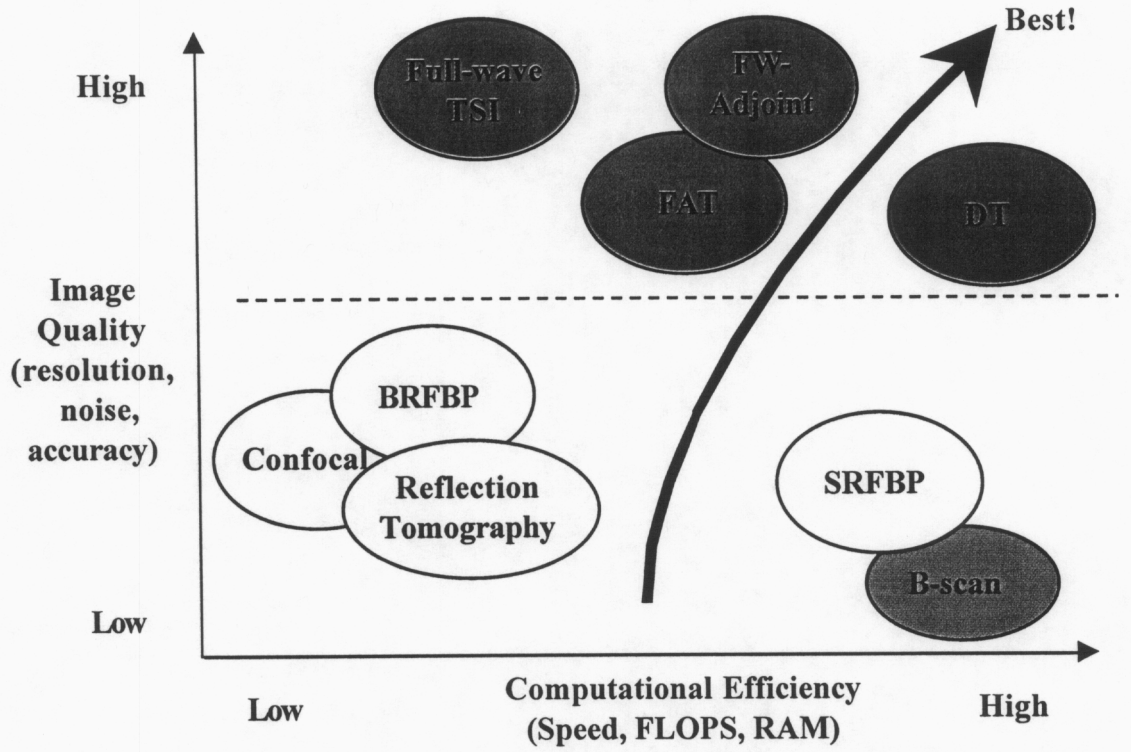

Figure 4.5.1 Illustration of the trade-off between computer requirements and quality of resolution, signal to noise, and quantification accuracy of sound speed and attenuation for many of the potential ultrasound reconstruction algorithms considered in this work. LLNL research and development goal for tissue imaging is both high quality and

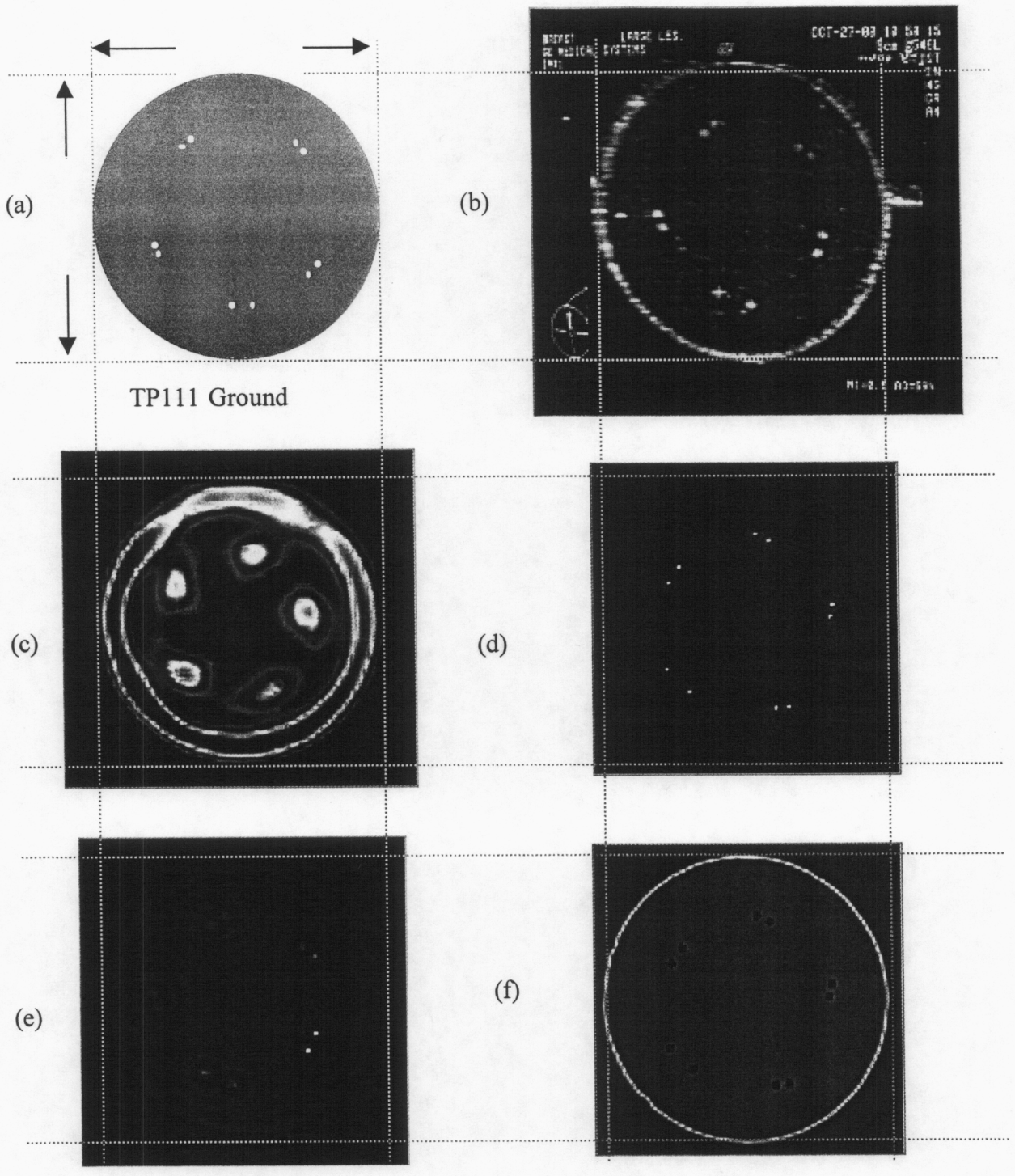

Figure 5.1.1 TP111 image reconstruction results with ground truth (a), 5 pairs of 0.2mm wires at 12.5mm from phantom center, (b) Medical B-scan (6-11Mhz) GE Logic 600, (c) Straight Ray Filtered BP (SRFBP), (d) Full aperature Tomography (FAT) with 0.4mm resolution, (e) Diffraction tomograpy (DT) with 0.7mm resolution and (f) TSI full wave algorithm with 0.5mm resolution. (grid overlay is not part of any reconstruction)

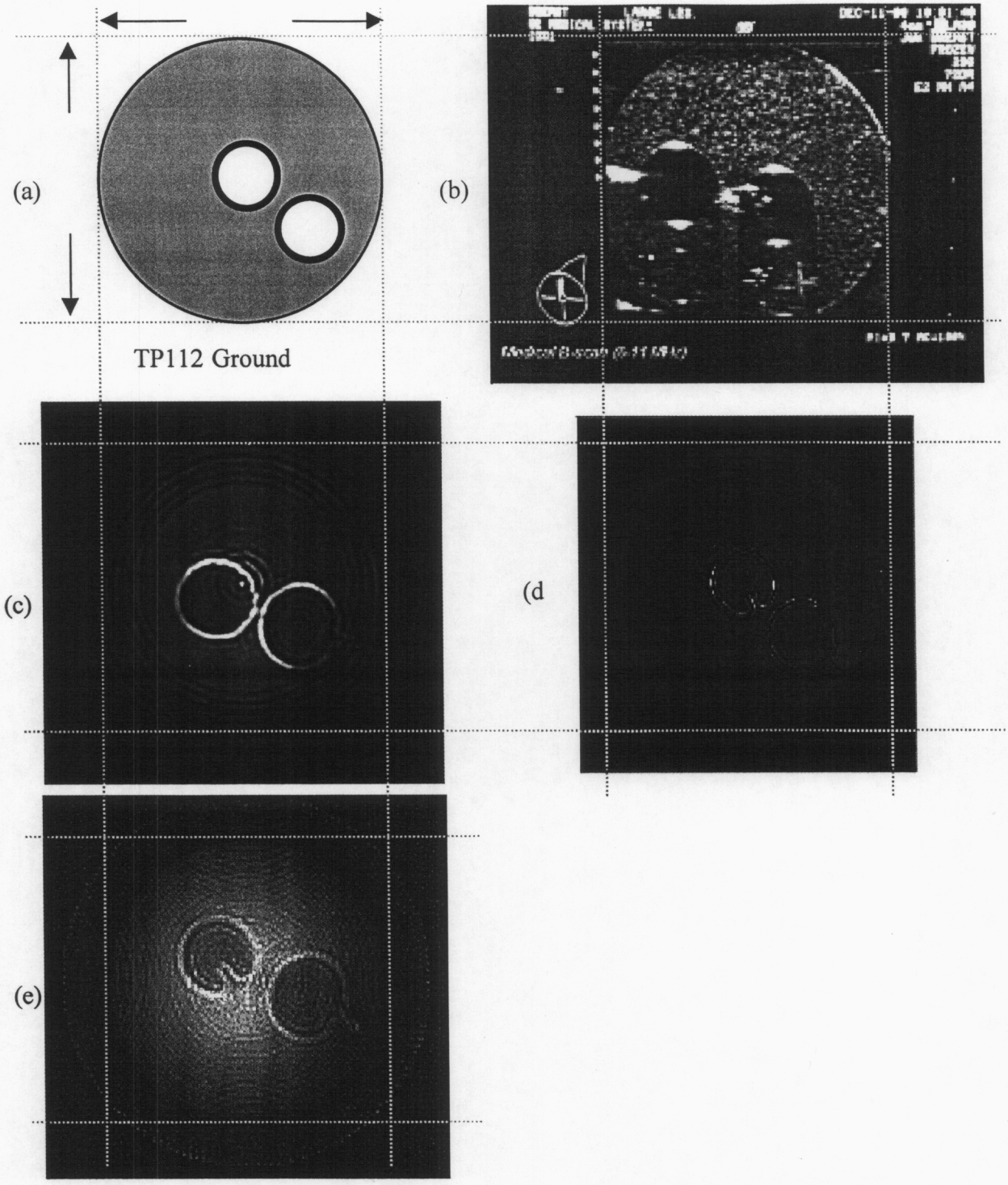

ground truth (a) indicates two10mm inclusions (water/alcohol
ical B-scan (6 - 11Mhz) GE Logic 600, (c) Diffraction tomograpy (DT) (0.6 MHz.), (d) Full aperature Tomography (FAT) with 0.4mm resolution (1.5 MHz.), and (e) TSI full wave algorithm with 0.5mm resolution (1.5 MHz.) . (grid overlay is not part of any reconstruction)

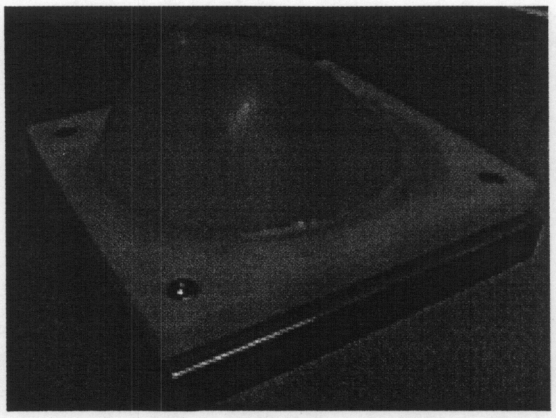

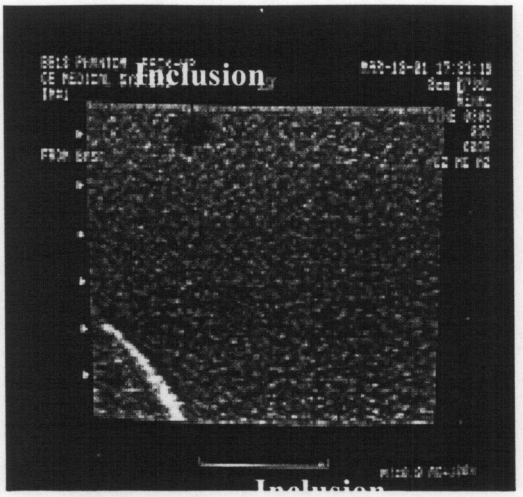

(a)

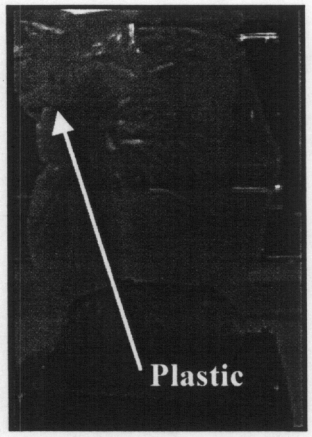

(b)

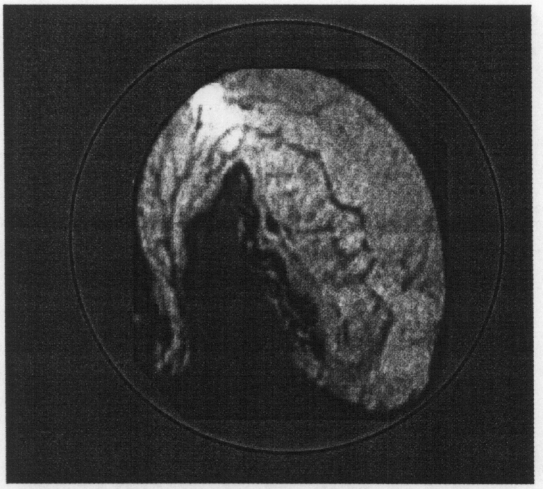

(c)

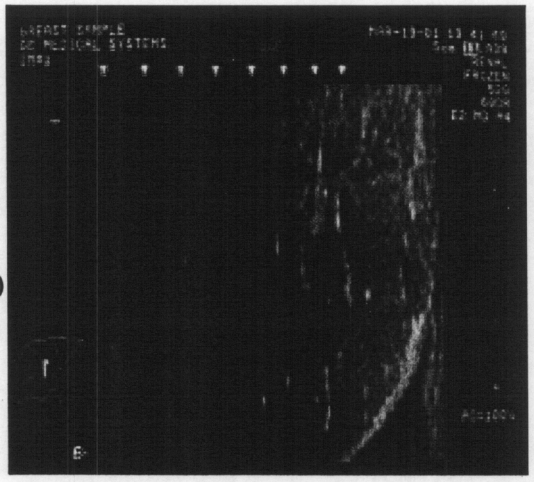

(d)

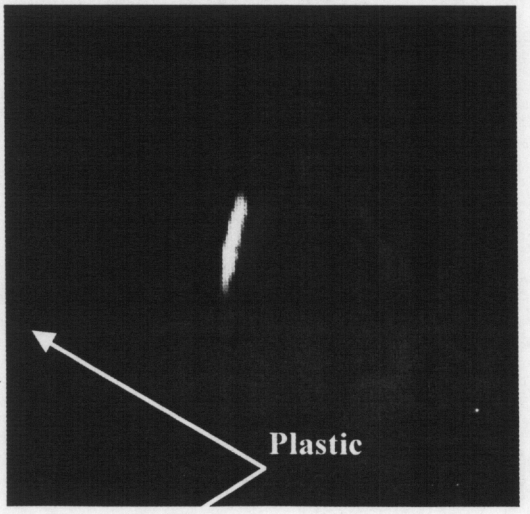

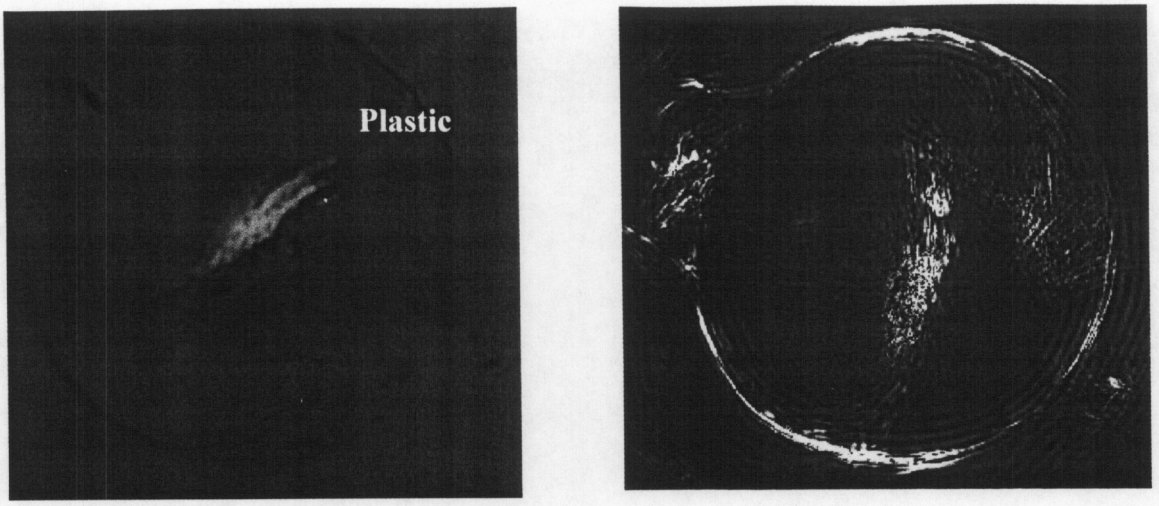

Figure 5.4.1 BTS1, a cadaveric breast placed in formalin and sealed in a 100mm container which was then inserted in a plastic bag and tied at the top (a). Cropped CT scan slice image showing the 'C' shape of the tissue (b). GE logic 600 reaults (c) . Plastic bag knot as well as the container edge could be seen in FWA, DT, and FAT (d, e, f). Somewhat of the 'C' shape can also be seen in the FWA (d) and FAT (f) images. Resolution is poor for all of the images.

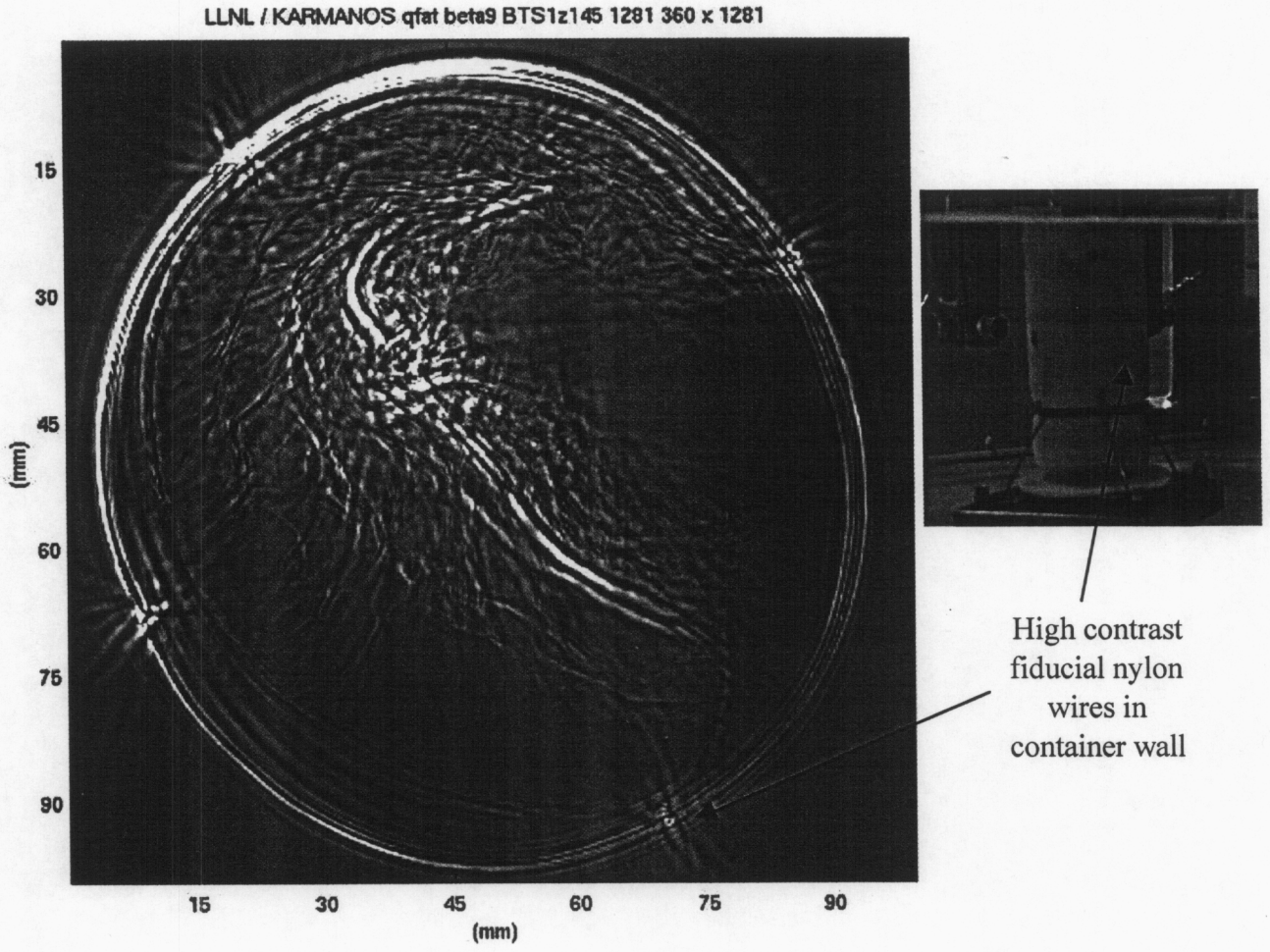

Figure 5.4.2 Removing the plastic bag improved resolution significantly. FAT reconstruction is shown here. Fiducial markers are clearly seen. Tissue striations and details <= 1mm are now discernible. Formalin areas are highly homogeneous and have few artifacts. The 'C' shape of the tissue is quite obvious.

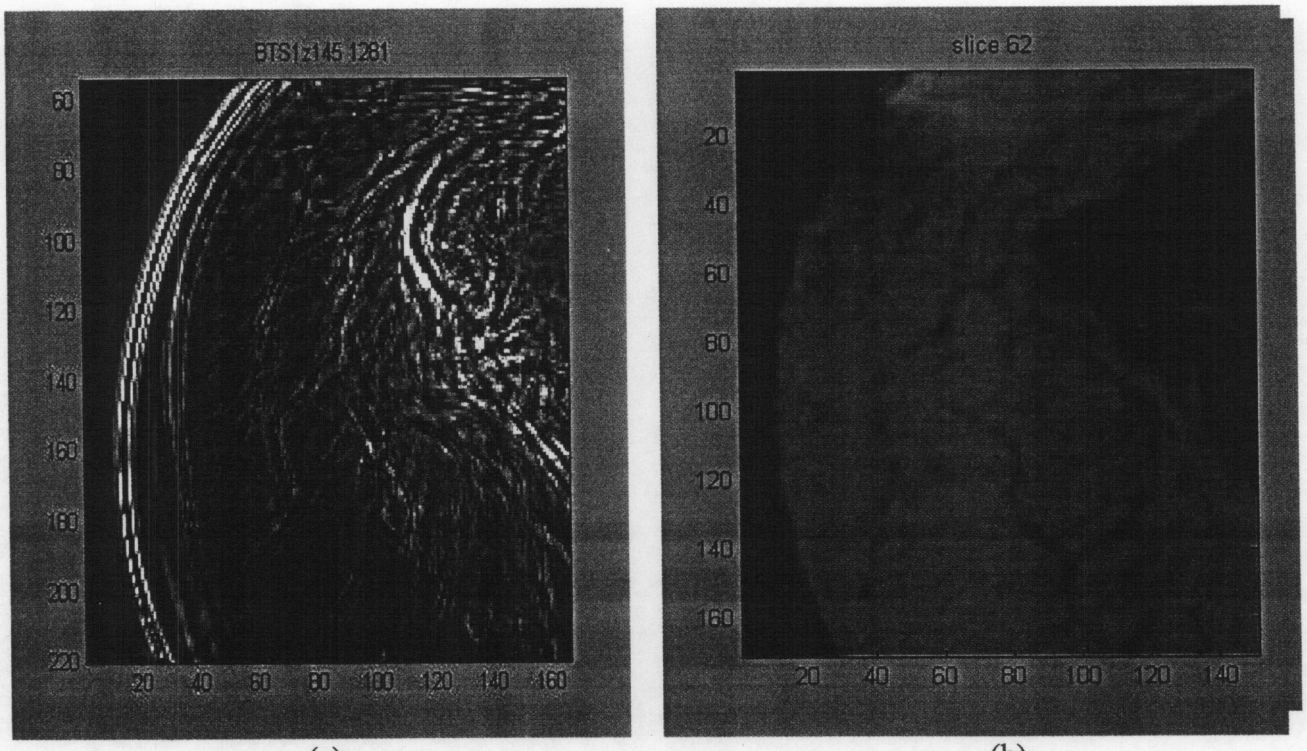

(a) (b)

Figure 5.4.3 (a) LLNL Full aperature tomography (FAT) reconstruction of BTS1 cadavaric breast tissue sample. 150 x 150 mm segment of reconstuction image is shown for close-up comparison. (b) UC Davis Medical Center x-ray CT reconstructon slice of approximately the same area in the tissue sample.